BIOFUNCTIONALIZATION OF Ti6Al4V SURFACE WITH Ag MODIFIED HAp COATINGS *VIA* ELECTROCHEMICAL DEPOSITION

Elena UNGUREANU[1], Ionut C. IONESCU[2], Raluca I. ZAMFIR-ANDRONIC[3], Marius VASILESCU[4], Claudia Georgiana MILEA[5], Mircea DOBRESCU[6], Diana M. VRANCEANU[7], Cosmin M. COTRUT[8,9]

The current study aim is to biofunctionalized the Ti6Al4V medical alloy with undoped (HAp) and Ag doped hydroxyapatite (Ag-HAp) coating by pulsed electrochemical deposition. The morphology of HAp has modified after Ag addition, revealing a surface made from thinner and wider plate crystals, on which small bright particles attributed to Ag were noted. Ag addition has increased the Ca/P ratio up to 1.62 from 1.58 in the case of undoped HAp. XRD and FTIR analysis have confirmed that both coatings consist in HAp phase and that the Ca from HAp structure was partially substituted by Ag. Nevertheless, the electrochemical measurements and in bioactivity assays, showed that the proposed coatings are enhancing the behavior of Ti6Al4V in simulated media, indicating their potential as biomaterials for medical applications.

Keywords: titanium alloys, biofunctionalization, electrochemical deposition, hydroxyapatite

1. Introduction

Ti6Al4V is the most widely used α+β Ti alloy in medical applications as implantable material, due to its higher mechanical strength and comprehensive

[1] PhD Student, Faculty of Materials Science and Engineering, University POLITEHNICA of Bucharest, Romania, e-mail: ungureanu.elena14@yahoo.com
[2] PhD Student, Faculty of Materials Science and Engineering, University POLITEHNICA of Bucharest, Romania, e-mail: ionescu.ionut.cornel@gmail.com
[3] Lecturer, Faculty of Materials Science and Engineering, University POLITEHNICA of Bucharest, Romania, e-mail: raluca.zamfir@upb.ro
[4] Lecturer, Faculty of Materials Science and Engineering, University POLITEHNICA of Bucharest, Romania, e-mail: lucian.vasilescu@upb.ro
[5] Assistant Prof. PhD student, Faculty of Materials Science and Engineering, University POLITEHNICA of Bucharest, Romania, e-mail: georgiana.milea@upb.ro
[6] Associated Prof., Faculty of Materials Science and Engineering, University POLITEHNICA of Bucharest, Romania, e-mail: mircea.dobrescu@upb.ro
[7] Lecturer, Faculty of Materials Science and Engineering, University POLITEHNICA of Bucharest, Romania, e-mail: diana.vranceanu@upb.ro
[8] Associated Prof., Faculty of Materials Science and Engineering, University POLITEHNICA of Bucharest, Romania, e-mail: cosmin.cotrut@upb.ro
[9] SR II, Dr. Eng., National Institute of Research and Development for Optoelectronics - INOE 2000, Măgurele, Romania, e-mail: cosmin.cotrut@upb.ro

performance [1,2]. However, long-term implantation of Ti6Al4V alloy triggers safety concerns due to the release of V and Al ions which are found to be associated with Alzheimer disease, neuropathy and osteomalacia [3]. In addition, the mismatch in the elastic moduli between α+β Ti alloy and cortical bone can lead to a loose interface at the implant-native bone level or to bone resorption, functional degradation, and even implant failure resulting from the incomplete load transfer between the implant and neighboring bone. Generally, the release of metallic ions increases as the pH value decreases [4] especially upon implantation when the pH riches 5 and then recover to 7.4 within weeks [5]. In a study achieved by Höhn [6] was demonstrated that the release of Ti, Al and V ions has increased when the pH of the testing media (DMEM) has decreased for Ti6Al4V uncoated and coated with TiO_2-NP or hydroxyapatite. A merrier release was noted for the uncoated specimen than for the coated ones suggesting that the addition of a layer can enhance the electrochemical behavior of Ti6Al4V alloy.

Thus, to overcome this issue, one solution consists in coating the Ti6Al4V with calcium phosphates-based ceramic [7–12]. Among most popular and studied bioceramic is hydroxyapatite (HAp) due to its resemblance to organic one which is found as main inorganic phase in hard bone tissue [8,13] HAp is a very versatile material due to its excellent properties in terms of biocompatibility, bioactivity, osseoconductivity but also because it can be tuned by addition of different other biocompatible elements such as Mg, Sr, Mn, Si, Fe, Zn etc.[14–20].

Currently, antibiotic prophylaxis is not sufficient for the treatment of infections associated with implantable materials. Thus, with respect to nowadays trends and conditions [21], a logical solution to overcome infections associated with implants failure [22,23] is to develop new alternatives, complementary to traditional pharmaceutical method.

Inorganic antimicrobial materials consist in metallic ions with biocide action added into synthetic HAp [24–27]. Among the metals which can be used for doping, silver (Ag) evidenced itself due to very good antimicrobial properties [25,28–30]. Incorporation of silver during the synthesis process involves the silver substitution for calcium, which may result in a Ca-deficient hydroxyapatite [27,31]. Silver exhibits good thermal stability, low volatility, is biocompatible and non-toxic to human cell at low concentration along with superior antibacterial characteristics [32,33]. According to Ref's. [34,35] Ag^+ ions interact with protein and enzymes of bacteria which result in structural damage of the cell membrane and death of bacterial cells, Ag^+ ion also disrupt the reproduction of bacteria by penetrating into the cell membrane bind itself to bacteria DNA and RNAs and inhibiting bacterial replication. Obtaining these properties in materials commonly used for surgical implants can be achieved through surface modification techniques that allow coating of the devices' surface, which is the first part to have contact with the biological environment [36–41]. Several means of obtaining HAp

based coatings on metallic substrate are reported in the literature of which electrochemical deposition [42] have attracted much interest in the past years due to its versatility. Thus, the aim of the present paper consists in enhancing to physico-chemical properties of hydroxyapatite-based coatings though addition of Ag by pulsed electrochemical deposition on Ti6Al4V substrate.

2. Materials and Methods

2.1. Materials

Substrate preparation

The electrochemical deposition of the coatings was made on Ti6Al4V alloy (grade 4, ELI, purchased from Bibus Metals AG, Germany) as discs of 20 mm diameter and 2 mm thickness. The samples were prepared on silicon carbide paper (320-800 grit) and cleaned with distilled water and izo-propylic alcohol. Before the electrochemical deposition, the substrates were sonicated in acetone to remove the residues or greases from the material surface.

Coating preparation

The coatings were prepared by pulsed electrochemical deposition (PED). The deposition was carried out in a standard electrochemical cell with the following configuration: reference electrode (RE) – saturated calomel electrode (SCE); auxiliar electrode (Aux. E) – a platinum plate electrode and the working electrode (WE) that consisted of Ti6Al4V alloy which was fixed in a Teflon holder. The electrochemical deposition was made with a multichannel Potentiostat/Galvanostat (Parstat MC, Princeton Applied Research - Ametek) by pulsing the potential for a specific time interval. The electrolyte used for the synthesis of the coatings is presented in Table 1.

Table 1.

Chemical composition of the electrolyte and sample codification

Coating type	Codification	Chemical composition			Ca/P ratio
		$Ca(NO_3)_2 \cdot 4H_2O$	$NH_4H_2PO_4$	$Ag(NO_3)$	
Ti6Al4V coated with hydroxyapatite	**HAp**	5 mM	3 mM	-	1.67
Ti6Al4V coated with silver doped hydroxyapatite	**Ag-HAp**	4.85 mM		0.15 mM	

Briefly, $Ca(NO_3)_2 \cdot 4H_2O$, $NH_4H_2PO_4$ and $Ag(NO_3)$ of analytical grade purchased from Sigma Aldrich (Germany) were dissolved in ultra-pure water (ASTM I, Millipore). The pH was adjusted to 4 by dropwise addition of 1M HNO_3 solution. The main parameters used for electrochemical deposition of the coatings are presented in Table 2. The employed technique consisted in two stages: 1) activation and 2) relaxation, that together form 1 cycle. During

activation stage, a potential (E_{ON}) was applied for a specific time (t_{ON}), while during the relaxation, noted with "OFF", the potential was null (0 V).

In the present study, the relaxation time was doubled compared to activation time, because at the interface electrolyte – substrate (Ti6Al4V), the concentration of the necessary ions can be reduced during deposition, leading to the formation of nonuniform coatings or other type of defects. Thus, by continuously stirring the electrolyte coupled with a prolonged relaxation time, the required ions for the deposition can be refilled, allowing the deposition of a uniform coating on the substrate.

Table 2.

Experimental conditions and main electrochemical parameters

Experimental conditions		HAp	Ag-HAp
Pulsed electrochemical deposition	**E_{ON}; t_{ON}**	-2 V; 0.5 s	
	E_{OFF}; t_{OFF}	0 V; 1 s	
	Deposition time (min)	90 min	10 min
	Deposition temperature	75 °C	

Compared to our previous study [43] in this study we have enhanced the coatings properties by modifying the electrochemical parameters involved in the deposition process. Before selecting the suitable electrochemical parameters for the undoped and Ag doped HAp coatings, several tests were performed with the aim of obtaining coatings with comparable thickness. The thickness of the coatings was determined by Dektak 150 stylus profilometer (stylus radius of 2.5 µm), by measuring the forming ledge between the deposited film and the uncoated substrate. The undoped HAp coatings presented a thickness of 6.7 µm, while for the Ag-HAp coatings, the deposition time was adjusted until the targeted thickness was attained. Based on the experimental design (Fig. 1), it was observed that Ag addition generates a higher deposition rate and therefore, the deposition time for the Ag/HAp coatings was reduced to 10 min. After deposition, the samples were cleaned with ultra-pure water and dried in a desiccator at room temperature.

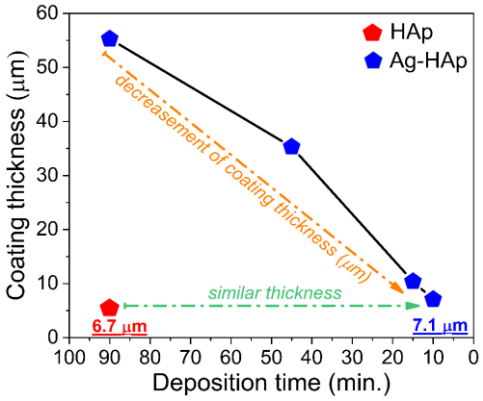

Fig. 1. Optimization of the electrochemical parameters with respect to coating thickness

2.2. Characterization

The coatings morphology and elemental composition was investigated with a scanning electron microscope (SEM) equipped with energy dispersive spectrometer (EDS) (Phenom ProX, Phenom World, Netherlands).

The microstructure of the coatings was determined by grazing-incidence X-Ray Diffraction (XRD) using a CuK_α radiation (SmartLab, Rigaku, Japan) from 20 to 80˚ with a step size of 0.02 ˚/min and an incident angle of 3˚.

The chemical bonds of the coatings were evidenced by Fourier Transform Infrared Spectroscopy at a resolution of 4 cm^{-1}, over the frequency 550 – 4000 cm^{-1}, using a spectrophotometer FT-IR, Jasco 6300 (Jasco, Japan) with universal ATR sampling accessory Pike MIRacle.

Surface roughness was measured over a length of 4 mm using a DEKTAK 150 (Veeco Instruments, USA) stylus profilometer, while the surface topography was carried out with an atomic force microscope (AFM, INNOVA, Veeco, USA), operating in tapping mode using 30 x 30 μm^2 area scans.

Electrochemical behavior of the proposed coatings was investigated at 37 ± 0.5 °C in two simulated media that mimic the human environment as human plasma (simulated body fluid – codified as SBF) and saliva (Fusayama artificial saliva – codified as Fusayama A.S.) using a PARSTAT 4000 Potentiostat/Galvanostat (Princeton Applied Research, USA) equipped with a low current interface module (LCI, Princeton Applied Research). Moreover, the electrochemical cell was introduced in a Faraday cage to eliminate possible interferences caused by electromagnetic fields. The chemical compositions of the used testing media are presented in Table 3.

Table 3.

Chemical composition of the simulated media: A) Simulated Body Fluid and B) Fusayama Artificial Saliva

A) SBF		**B) Fusayama A.S.**	
Reagent	**Amount**	**Reagent**	**Amount**
NaCl,	8.035 gL^{-1}	NaCl,	0.4 gL^{-1}
$NaHCO_3$	0.350 gL^{-1}	KCl,	0.9 gL^{-1}
NaCl,	0.225 gL^{-1}	urea,	1 gL^{-1}
$K_2HPO_4 \cdot 3H_2O$	0.231 gL^{-1}	NaH_2PO_4	0.69 gL^{-1}
$MgCl_2 \cdot 6H_2O$	0.311 gL^{-1}	$CaCl \cdot 2H_2O$	0.795 gL^{-1}
1 M-HCl	39 mL	$Na_2S \cdot 9H_2O$	0.005 gl^{-1}
$CaCl_2$	0.292 gL^{-1}		
Na_2SO_4	0.072 gL^{-1}		
$(CH_2OH)_3CNH_2$	6.118 gL^{-1}		
	*p*H 7.4		*p*H 5.2

On each examined sample, an area of 1 cm^2 was exposed to the electrolyte (SBF or AS). In all electrochemical measurements a typical three-electrode cell with the following set-up was used: Ti6Al4V as working electrode (WE),

platinum electrode was used as a counter electrode (CE) and saturated calomel (SCE) as reference electrode (RE). The tests were achieved according to the ASTM G5–14e1 standard at a scanning rate of 0.167 mV/s. The open circuit potential (OCP) was monitored for 1 h, starting right after the sample's immersion in the electrolyte and the potentiodynamic curves were recorded from − 1 V vs. OCP to +1 V vs. SCE.

In vitro bioactivity tests were performed to evaluate the coatings ability to form new apatite precipitates in SBF. The samples were immersed for 21 days in SBF (chemical composition is presented in Table 3A) at human body temperature (37 ± 0.5 °C) in an incubator (Memmert IF 55, Memmert GmbH, Germany). The testing SBF media was renewed daily to prevent chemical exhaustion and to eliminate the possibility of bacteria/microorganisms' growth. The mass of apatite formed on the exposed surface was monitored using an analytical balance having an accuracy of 0.01 mg. The weight variation of the formed apatite on the surface was determined using the following equation:

$$\Delta m = \frac{m_f - m_i}{mi} \cdot 100\ [\%] \quad (1)$$

where: Δm – is the apatite mass formed on the surface in percentages, m_i and m_f are the sample weight before and after exposure to SBF, correspondingly. After removing the samples from SBF media and before weighting, all samples were rinsed in distilled water and dried in the desiccator for 24 h to remove the water from their structure. The *in vitro* bioactivity results for the coated and uncoated samples are presented in terms of evolution of the newly formed apatite. Moreover, the morphology of the newly formed apatite was highlighted through scanning electron microscopy (Phenom ProX, Phenom World, Netherlands).

3. Results and discussions

3.1. Morphology and elemental composition

In Fig. 2, there are presented the SEM images acquired on the developed coatings. At smaller magnification, was observed that both coatings are compact and uniform, and are covering the entire investigated surface. For Ag-HAp present some small agglomerations, which can be attributed to addition of Ag. At higher magnification, the morphology of simple HAp coatings is made of thin plate like-crystals. In the case of Ag-HAp coatings was noted that after addition of Ag, the morphology consists in thinner and wider plate like crystals, on which small bright particles, attributed to Ag, are fixed. Thus, it can be assumed that the observed agglomerations, are silver nanoparticles, obtained during the deposition process [44]. According to a study performed by Sharma et al. [45] Ag nanoparticles may be more efficient than Ag^+ ions in performing antimicrobial activities.

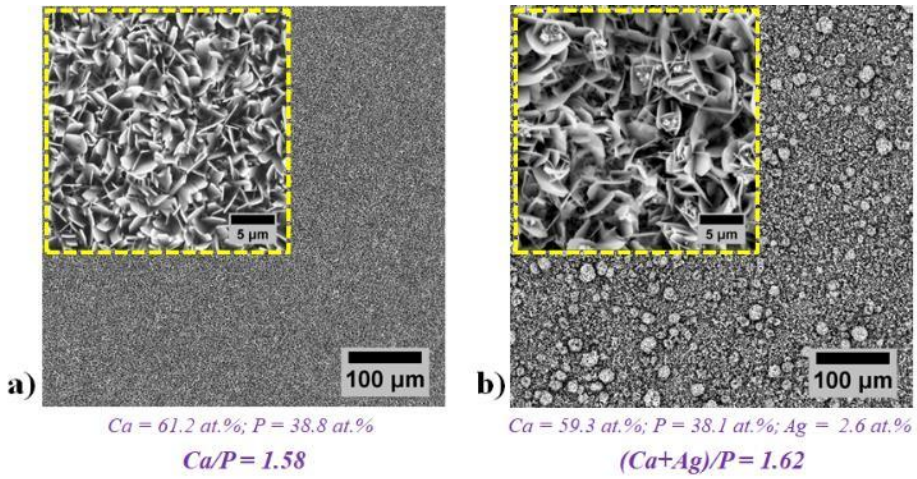

Fig. 2. SEM images and chemical composition of (a) HAp and (b) Ag-HAp coatings obtained by pulsed electrochemical deposition technique

The chemical composition achieved on the coatings evidenced the presence of the characteristic elements of HAp (Ca and P) and the doping element (Ag). The C/P ratio calculated was of 1.58 for simple HAp and 1.62 for the Ag-HAp coatings, indicating that addition of Ag has a beneficial effect by slightly increasing the ratio. Both coatings registered ratios slightly lower than the one of stoichiometric HAp (1.67).

3.2. Phasic composition

The obtained XRD patterns of the coatings are presented in Fig. 3. One can see that the developed coatings are crystalline. No other calcium phosphate (CaP) based phases were identified. The peaks of both coating were associated to standard HAp (ICDD, #09-0432). After Ag addition the crystallinity of HAp has decreased, this being noted for the relative intensity of (002) peak, registering smaller values, which is found to be in good agreement with the literature [46]. Ag incorporation into the HAp lattice, shifted the diffraction peaks to lower 2θ values [43], denoting an expansion in the crystal lattice. This can be explained by the radius differences between Ag^{+} (0.126) and Ca^{2+} (0.99 nm) [47,48].

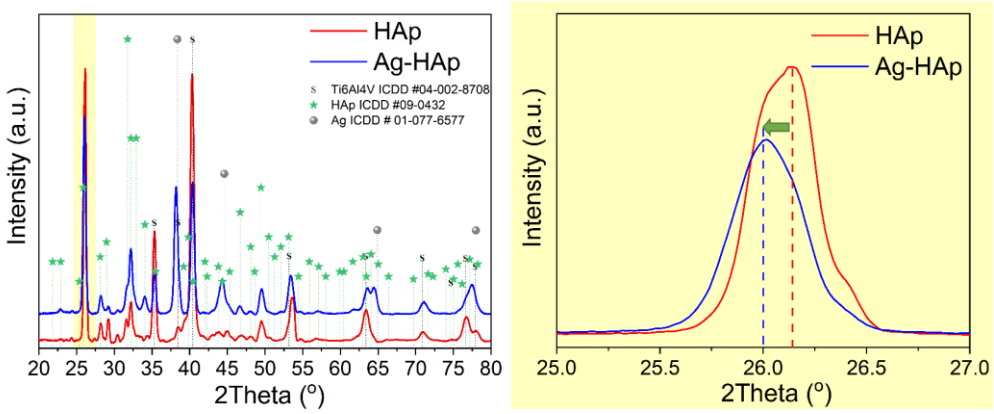

Fig. 3. XRD pattern of the HAp and Ag-HAp coatings electrochemically deposited on Ti6Al4V

XRD analysis also revealed the presence of some diffraction peaks that correspond to Ag metallic (ICCD, #01-077-6577), pointing out that not all the silver was incorporated in the HAp. According to a study performed by Pishbin [49], addition of $AgNO_3$ can lead to formation of Ag nanoparticles, of whose reflection on XRD spectra can be attributed to metallic Ag (cubic crystalline structure). These findings are in good agreement with SEM analysis in which agglomeration of small and bright nano-particles were observed and attributed to Ag. The size of HAp crystallites was calculated from (002) reflection in XRD pattern using the Scherrer approximation (Eq.2) and the obtained results are presented in Table 4.

$$d_{(002)} = \frac{k\lambda}{\beta cos\theta} \quad (2.)$$

Table 4.

Lattice parameters, crystallite dimension and crystallinity calculated for the developed coatings

Sample	Lattice parameter		Crystallite dimension d[nm]
	a = b	c	
Standard HAp	**9.41 Å**	**6.85 Å**	-
HAp	9.51 Å	6.85 Å	35.88
Ag-HAp	9.62 Å	6.85 Å	21.23

where d_{hkl} is the crystallite size, as calculated from (002) reflection, λ is the wavelength of Cu-K_α radiation (1.5406 Å), β is full width at half maximum intensity of the peak along (002) direction and k is the broadening constant with crystal habit (0.9 for elongated apatite crystals). As shown in Table 4, the coatings have similar values to standard HAp for *c* axis, while *a* axis presents some higher values, suggesting that some small modifications of HAp lattice have occurred. This is more pronounce after Ag addition, when the value has increased from 9.51 Å registered for undoped HAp to 9.62 Å for the Ag-HAp coating. The crystallite dimension calculated for undoped HAp was of ~ 36 nm and has decreased after

Ag addition to ~ 21 nm, which is found to be in good agreement with other studies [50].

3.3. Roughness and topography

Roughness is a critical parameter which can influence the materials electrochemical behavior and its interaction with the human cells. Thus, it is reasonable to assume that by controlling this parameter some surface characteristics can also be enhanced. In table 5 are presented the main roughness parameters extracted from coating profiles.

As a new trend, the changes of surface roughness at the nanoscale level seem to strongly influence the host response at both cellular and tissue levels [51]. In this context, strategies such as electrochemical deposition were developed to obtain significant nano-topographies coating when compared to other HAp techniques. According to the obtained results, it can be observed that in contrast with Ti6Al4V substrate, which exhibits a flat topography (Ra=28 nm), the coatings presented values of ~ 200 nm for HAp and of ~ 900 nm for Ag-HAp. Based on this founding it can be assumed that the higher roughness obtained for Ag-HAp coatings is due to the Ag agglomerations.

Table 5.

The main roughness parameters of the developed coatings

Samples	Roughness parameters		
	Ra [nm]	Rq [nm]	Skw
Ti6Al4V	28.6 (±3.5)	36.1 (±3.7)	-0.1 (±0.02)
HAp	198.4 (±11.2)	253.7 (±18.4)	+0.41 (±0.08)
Ag-HAp	889.9 (±59.5)	1108.2 (±70.7)	+0.74 (±0.12)

It is known that the morphological features, such as surface roughness and topography, can strongly influence protein adsorption, cell attachment, proliferation and differentiation [52]. Fig. 4 shows the surface topography of HAp and Ag-HAp coatings deposited on Ti6Al4V.

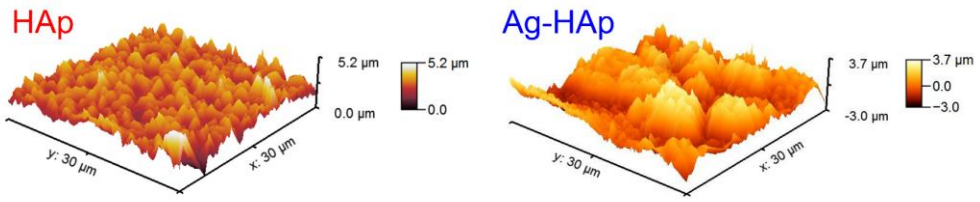

Fig. 4. AFM topographies of the developed coatings

As it can be seen, the HAp crystals are different in their size and shape. After, Ag addition, the crystals are larger with sharper edges, compared with undoped HAp which presents much smaller and regular crystals.

3.4. Chemical bonds

The FTIR spectra of the HAp and Ag-HAp coatings is presented in Fig. 5 Even though no significant distinction between the HAp and Ag-HAp coatings were noted, some minor modification in terms of intensities of the individual bands were observed, suggesting that the presence of Ag affects the structure of HAp [53].

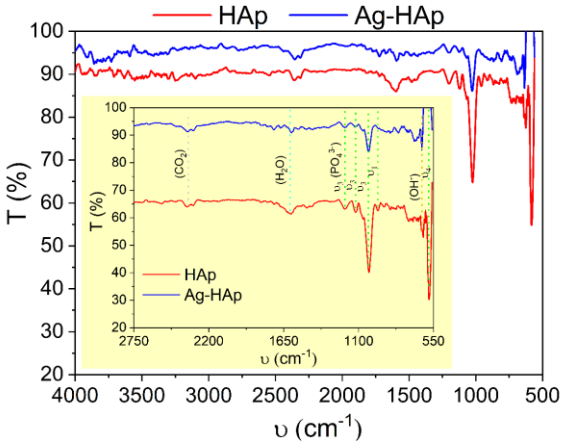

Fig. 5. FTIR spectra of the obtained coatings

Both spectra show the characteristics bands for phosphate group $(PO_4)^{3-}$ in the range 900-1200 cm^{-1} (triply degenerated asymmetric stretching mode, v_3, and symmetric stretching mode v_1, of the P-O bonds) [28,54].

The FTIR spectra of both coatings include a well-defined peak at 1020 cm^{-1} with one shoulder at 1080 cm^{-1}, which is characteristic for HAp [55,56] and were assigned to ν_3 asymmetric stretching of $(PO_4)^{3-}$. The ν_1, ν_3 and ν_4 vibrations are considered the IR fingerprints of HAp structure and their presence indicate the formation of an apatite structure. Compared to undoped HAp, after Ag addition the $(PO_4)^{3-}$ bands presented smaller intensities suggesting that the HAp structure might present some alterations. The peak at 630 cm^{-1} is characteristic for OH^- structural and proves the presence of HAp [33]. Nevertheless, at 1650 cm^{-1} the H_2O band was noted [57] while the peak at ~ 2300 cm^{-1} is an indicative of the atmospheric CO_2^{-3} from the IR chamber [8]. Due to the porosity and roughness of the coatings, the spectra present "noises" and did not make possible the identification of other peaks, such as the Ag-O bonds.

3.5. Electrochemical measurement

The electrochemical behavior of the coatings was evaluated through polarization resistance technique in two simulated media whose chemical composition can be found in Table. 3. These two media were selected because the proposed coatings can be used in both orthopedy and dentistry field - SBF resemblance to human plasma while Fusayama mimics the natural saliva.

In Fig. 6, there are presented the potentiodynamic curves registered for both coatings and the substrate, which was considered as reference sample in SBF and Fusayama artificial saliva. From Tafel extrapolation the main electrochemical parameters were extracted (E_{corr} – corrosion potential and i_{corr} – corrosion current density) and in Table 6 are presented.

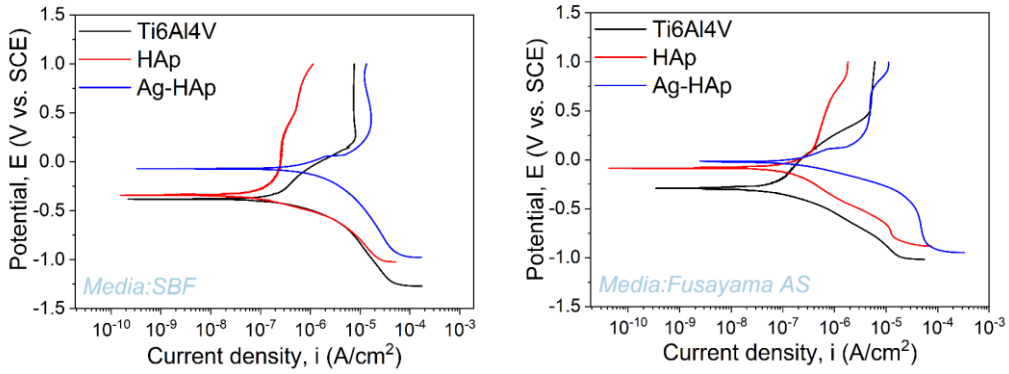

Fig.6. Potentiodynamic polarization curves of the uncoated and coated Ti6Al4V substrates in SBF and Fusayama artificial saliva

Table 6.

Electrochemical parameters of the investigated samples

Sample	Electrolyte	E_{OCP} [mV]	E_{corr} [mV]	i_{corr} [nA/cm^2]
Ti6Al4V	**SBF**	- 286.01	- 283.37	83.75
HAp		- 7.13	- 206.28	40.07
Ag-HAp		- 10.58	- 56.64	780.80
Ti6Al4V	**Fusayama AS**	-22.15	- 292.95	96.13
HAp		115.32	- 81.81	60.71
Ag-HAp		74.07	- 21.88	232.27

Regarding the electrolytes composition it is worth mentioning that the major difference between them is given by the chloride ions concentration, which is higher in SBF, compared to Fusayama. It is known, that a material is resistant to the corrosive attack of a media when it is has a more electropositive corrosion potential (E_{corr}) and a low corrosion current density (i_{corr}) [58].

The electrochemical behavior tests show that:

- regardless the testing media, both coated samples exhibited more electropositive corrosion potentials (E_{corr}) than uncoated ones;
- by comparing the coatings, one can see that irrespective of the testing media, addition of Ag has led to a more electropositive E_{corr} and highest i_{corr} values, which could be due to the metallic character of Ag and may indirectly indicate that the Ag ions can be released in the environment and thus fulfilling their purpose;

– compared to SBF media, in Fusayama artificial saliva, the obtained values are smaller, indicating that the corrosive process are not so energetic.

Thus, the electrochemical tests have highlighted that in order to prevent the toxic ions release, the corrosion resistance of Ti6Al4V substrate can be enhanced with undoped and Ag doped HAp based coating. Moreover, the obtained values indicate that the proposed coatings are suitable for orthopedic and dental applications.

3.6. Biomineralization in SBF

The *in vitro* biomineralization ability of a materials can be estimated by quantifying the newly formed apatite on the coatings.

The obtained coatings were immersed in SBF media for biomineralization ability evaluation of the developed materials. Each sample was immersed in 50 mL of testing media in sterilized containers in an incubator at 37 ˚C for 21 days. Each day the media was refreshed to assure the necessary ion concentration. At different time interval (1, 3, 7, 14 and 21 day) samples were removed and investigated in terms of surface morphology by SEM (Fig. 7) and mass variation (Fig. 8).

SEM images presented in Fig. 7 are showing that after 21 days of immersion in SBF media, all coated samples are predominantly covered in hemispherical precipitates with some cracks. Compared to undoped HAp, the Ag addition has favored the formation of hemispherical precipitated much earlier demonstrating, an accelerated biomineralization process. Thus, in the case of Ag-HAp coatings, after 7 days of immersion the semispherical features were covering the entire surface, while for the undoped HAp, the hemispherical precipitates begin to form and cover the surface after 14 days.

In Fig 8.a is presented a SEM image in cross-section for the undoped HAp coatings after 21 days of immersion in SBF media. As it can be noted, the thickness of the coating has increased to ~8 µm (± 0.7 µm) after immersion in SBF media, compared to its initial value of ~ 6.7 µm. Some plate-like crystals of the coating before immersion are still visible in the lower part of the coating. As already shown in our previous paper [15] the plate like-crystals and nano-walls create an abundance of pores, that favor the biomineralization process, leading to a thicker and compact layer of newly formed apatite.

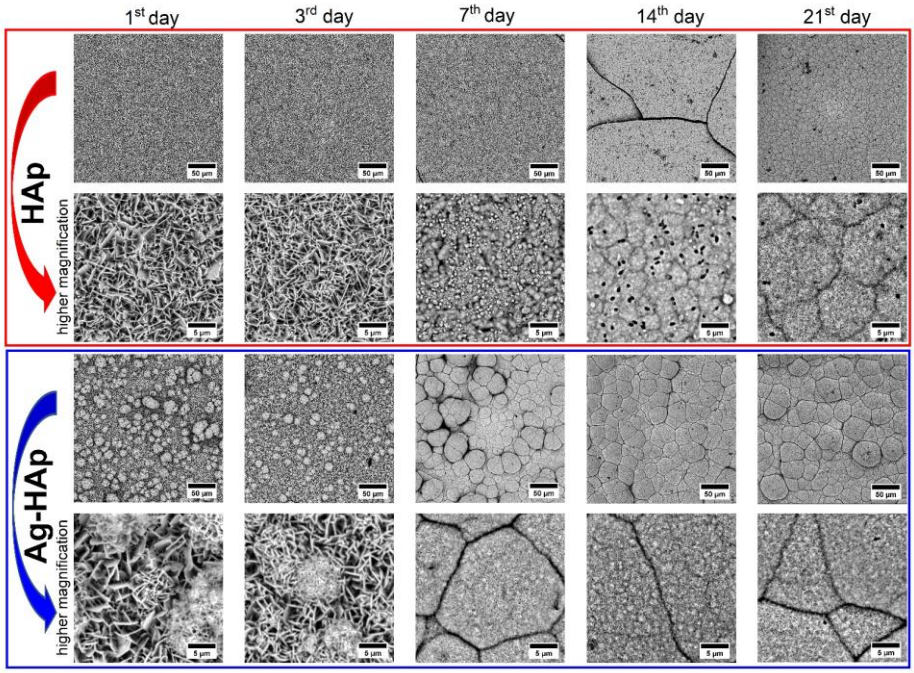

Fig. 7. SEM images of the HAp and Ag-HAp coating surfaces after immersion in SBF media

Fig. 8.b. reveals the mass dynamics of the investigated materials after 21 days of immersion in SBF. While the uncoated samples were not showing any significant additional mass, both coated samples acquired additional apatite quite rapidly.

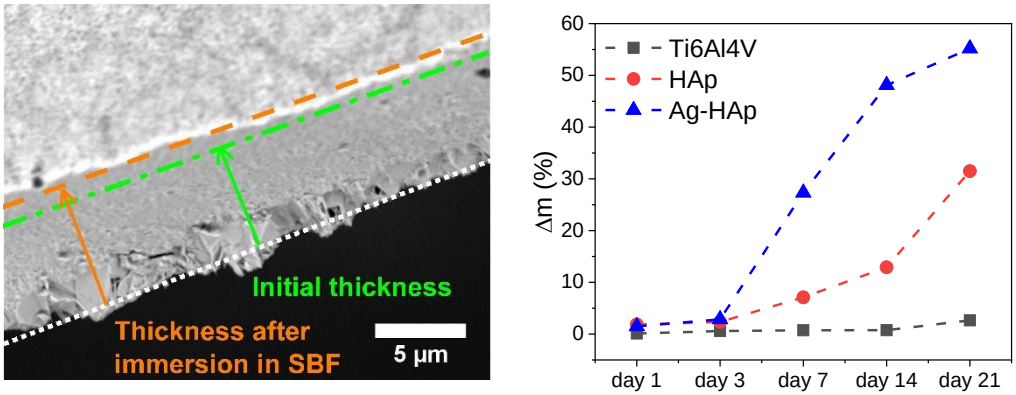

a) ***b)***

Fig. 8. a) Representative SEM image in cross-section of simple HAp coatings after 21 days of immersion in SBF media (green line and arrow – thickness of the HAp coating before immersion in SBF media; orange line & arrow – thickness of the coating after immersion in SBF media); b) Mass evolution of the newly formed apatite on HAp and Ag-HAp coatings

The highest biomineralization ability was found in the case of Ag doped HAp which after 21 days of SBF exposure has gain more than 55% than its initial value, while the undoped HAp has gained ~ 30%. Thus, based on this it can be stated that the biomineralization ability can be enhanced by Ag addition into the HAp structure.

4. Conclusions

In conclusion, the present study highlighted the following:

- electrochemical deposition of undoped and Ag doped HAp coatings on Ti6Al4V by pulsed electrochemical deposition was successfully achieved;
- both coatings are compact and uniform, and are covering the entire surface;
- the morphology of simple HAp coatings consists in thin plate like-crystals, which after addition of Ag, became thinner and wider plate like crystals; also, small bright particles, attributed to Ag, were noted;
- by addition of Ag, the Ca/P ratio was improved from a value of 1.58 to 1.62;
- XRD analysis has evidenced that both coatings presented the characteristic peaks of HAp; Ag addition has generated shifts towards smaller angles, indicating that Ca was partially substituted;
- both coatings have registered higher roughness than the substrate; by comparison, the Ag-HAp roughness is 5 times higher than HAp one;
- IR spectroscopy has evidenced the presence of the functional groups (PO_4^{3-}) indicating the formation of HAp;
- the coatings can improve the corrosion behaviour of the substrate, regardless the testing media (SBF or Fusayama AS), indicating that are suitable candidates for orthopaedic or dental applications;
- the biomineralization ability of Ti6Al4V alloy was improved by the undoped and Ag doped HAp based coatings; the highest mass increment was noted for the Ag-HAp coatings with a mass gain of ~55%, compared to ~ 30% registered for HAp.

Thus, the proposed coatings have overall enhanced the physico-chemical and electrochemical properties of Ti6Al4V substrate and, with respect to the medical application for which these coatings were designed, it can be said that the coatings features can be adjusted through addition of Ag.

Acknowledgments

The work was supported by the Operational Program Human Capital of the Ministry of European Funds through the Financial Agreement 51668/09.07.2019, SMIS code 124705; by the "Excellence Research Grants" Program, UPB – GEX, identifier: UPB–EXCELENTA–2016, project no. 54/2016 (PEDHAg) and through Romanian National Authority for Scientific Research and

Innovation CCCDI-UEFISCDI, project COFUND-ERANET EURONANOMED 3-NANO-VERTEBRA, within PNCDI III (no. 91/2019).

R E F E R E N C E S

[1] *M. Geetha, A. K. Singh, R. Asokamani, A. K. Gogia,* "Ti based biomaterials, the ultimate choice for orthopaedic implants – A review," in Prog. Mater. Sci., **Vol. 54**, Iss. 3, 2009, pp. 397-425.

[2] *C. M. Cotrut, A. C. Parau, A. I. Gherghilescu, I. Titorencu, I. Pana, D. V. Cojocaru, V. Pruna, L. Constantin, I. Dan, D. M. Vranceanu, A. Vladescu,* "Mechanical, in vitro corrosion resistance and biological compatibility of cast and annealed Ti25Nb10Zr alloy," in Metals, **Vol. 7**, Iss. 3, Article No. 86, 2017, pp. 1-23.

[3] *S. Nag, R. Banerjee, H. L. Fraser,* "Microstructural evolution and strengthening mechanisms in Ti–Nb–Zr–Ta, Ti–Mo–Zr–Fe and Ti–15Mo biocompatible alloys," in Mater. Sci. Eng. C, **Vol. 25**, Iss. 3, 2005, pp. 357-362.

[4] *M. Talha, Y. Ma, P. Kumar, Y. Lin, A. Singh,* "Role of protein adsorption in the bio corrosion of metallic implants – A review," in Colloids Surfaces B Biointerfaces, Vol. 176, 2019, pp. 494-506.

[5] *L. L. Hench, E. C. Ethridge,* "Biomaterials: the interfacial problem," in Adv. Biomed. Eng., **Vol. 5**, 1975, pp. 35–150.

[6] *S. Höhn, S. Virtanen,* "Effect of inflammatory conditions and H_2O_2 on bare and coated Ti–6Al–4V surfaces: Corrosion behavior, metal ion release and Ca-P formation under long-term immersion in DMEM," in Appl. Surf. Sci., Vol. **357**, 2015, pp. 101-111.

[7] *R. A. Surmenev, M. A. Surmeneva,* "A critical review of decades of research on calcium phosphate–based coatings: How far are we from their widespread clinical application?," in Curr. Opin. Biomed. Eng., **Vol. 10**, 2019, pp. 35-44.

[8] *N. Eliaz, N. Metoki,* "Calcium Phosphate Bioceramics: A Review of Their History, Structure, Properties, Coating Technologies and Biomedical Applications," in Materials, **Vol. 10**, Iss. 4, 2017, 334.

[9] *M. Saveleva, A. Vladescu, C. Cotrut, L. Van der Meeren, M. Surmeneva, R. Surmenev, B. Parakhonskiy, A. G. Skirtach,* "The effect of hybrid coatings based on hydrogel, biopolymer and inorganic components on the corrosion behavior of titanium bone implants," in J. Mater. Chem. B, **Vol. 7**, Iss. 43, 2019, 6778–6788.

[10] *L. Duta, C. Ristoscu, G. E. Stan, M. A. Husanu, C. Besleaga, M. C. Chifiriuc, V. Lazar, C. Bleotu, F. Miculescu, N. Mihailescu, E. Axente, M. Badiceanu, D. Bociaga, I. N. Mihailescu,* "New bio-active, antimicrobial and adherent coatings of nanostructured carbon double-reinforced with silver and silicon by Matrix-Assisted Pulsed Laser Evaporation for medical applications," in Appl. Surf. Sci., **Vol. 441**, 2018, pp. 871–883.

[11] *S. A. Adeleke, A. R. Bushroa, I. Sopyan,* "Recent development of calcium phosphate-based coatings on titanium alloy implants," in Surf. Eng. Appl. Electrochem., **Vol. 53**, Iss. 5, 2017, pp. 419–433.

[12] *J. V. Rau, I. Antoniac, G. Cama, V. S. Komlev, A. Ravaglioli,* "Bioactive Materials for Bone Tissue Engineering," in Biomed Res. Int., **Vol. 2016**, Article ID 3741428, 2016, pp. 1–3.

[13] *A. Maidaniuc, F. Miculescu, R. C. Ciocoiu, T. M. Butte, I. Pasuk, G. E. Stan, S. I. Voicu, L. T. Ciocan,* "Effect of the processing parameters on surface, physico-chemical and mechanical features of bioceramics synthesized from abundant carp fish bones," in Ceram. Int., **Vol. 46,** Iss. 8, pp. 10159-10171.

[14] *D. M. Vranceanu, A. C. Parau, C. M. Cotrut, A. E. Kiss, L. R. Constantin, V. Braic, A. Vladescu,* "In vitro evaluation of Ag doped hydroxyapatite coatings in acellular media," in

Ceram. Int., **Vol. 45**, Iss. 8, 2019, pp. 11050-11061.

[15] *A. Vladescu, D. M. Vranceanu, S. Kulesza, A. N. Ivanov, M. Bramowicz, A. S. Fedonnikov, M. Braic, I. A. Norkin, A. Koptyug, M. O. Kurtukova, M. Dinu, I. Pana, M. A. Surmeneva, R. A. Surmenev, C. M. Cotrut,* "Influence of the electrolyte's pH on the properties of electrochemically deposited hydroxyapatite coating on additively manufactured Ti64 alloy," in Sci. Rep., **Vol. 7,** Iss**.** 1, 2017, Article No. 16819.

[16] *I. V. Antoniac, M. Filipescu, K. Barbaro, A. Bonciu, R. Birjega, C. M. Cotrut, E. Galvano, M. Fosca, I. V. Fadeeva, G. Vadalà, M. Dinescu, J. V. Rau,* "Iron Ion- Doped Tricalcium Phosphate Coatings Improve the Properties of Biodegradable Magnesium Alloys for Biomedical Implant Application," in Adv. Mater. Interfaces, **Vol. 7**, Iss. 16, 2020, Article No. 2000531.

[17] *I. Cacciotti,* "Multisubstituted hydroxyapatite powders and coatings: The influence of the codoping on the hydroxyapatite performances," in Int. J. Appl. Ceram. Technol., **Vol. 16,** Iss. 5, 2019, pp. 1864–1884.

[18] *D. M. Vranceanu, I. C. Ionescu, E. Ungureanu, M. O. Cojocaru, A. Vladescu, C. M. Cotrut*, "Magnesium doped hydroxyapatite-based coatings obtained by pulsed galvanostatic electrochemical deposition with adjustable electrochemical behavior," in Coatings, **Vol. 10,** Iss. 8, 2020, Article No. 727.

[19] *J. V. Rau, I. V. Fadeeva, A. S. Fomin, K. Barbaro, E. Galvano, A. P. Ryzhov, F. Murzakhanov, M. Gafurov, S. Orlinskii, I. Antoniac, V. Uskoković,* "SiC Parvis Magna: Manganese-Substituted Tricalcium Phosphate and Its Biophysical Properties," in ACS Biomater. Sci. Eng., **Vol. 5,** Iss. 12, 2019, pp. 6632–6644.

[20] *A. Vladescu, C. Mihai Cotrut, F. Ak Azem, M. Bramowicz, I. Pana, V. Braic, I. Birlik, A. Kiss, M. Braic, R. Abdulgader, R. Booysen, S. Kulesza, T. K. Monsee*s, "Sputtered Si and Mg doped hydroxyapatite for biomedical applications," in Biomed. Mater., **Vol. 13,** Iss. 2, 2018, Article No. 025011.

[21] *A. Moldoveanu, O.-M. Ferche, F. Moldoveanu, R. G. Lupu, D. Cinteza, D. Constantin Irimia, C. Toader,* "The TRAVEE System for a Multimodal Neuromotor Rehabilitation," in IEEE Access, **Vol.** 7, 2019, pp. 8151–8171.

[22] *M. Bellantone, H. D. Williams, L. L. Hench,* "Broad-spectrum bactericidal activity of Ag_2O-doped bioactive glass," in Antimicrob. Agents Chemother., **Vol. 46,** Iss. 6, 2002, pp. 1940–1945.

[23] *M. Riaz, R. Zia, F. Saleemi, H. Ikram, F. Bashir,* "In vitro antimicrobial activity of ZnO based glass–ceramics against pathogenic bacteria," in J. Mater. Sci. Mater. Med., **Vol. 26**, Iss. 12, 2015, Article No. 268.

[24] *T. T. Tran, N. B. Nichita, M. O. Dobrica, C. M. Cotrut, M. D. Vranceanu, M. Tarcolea,* "In vitro biocompatibility investigation of silver and zinc modified hydroxyapatite deposited on implant materials," in UPB Sci. Bull. Ser. B Chem. Mater. Sci., **Vol. 82**, Iss. 3, 2020, pp. 231–245.

[25] *S. Ciuca, M. Badea, E. Pozna, I. Pana, A. Kiss, L. Floroian, A. Semenescu, C. M. Cotrut, M. Moga, A. Vladescu,* "Evaluation of Ag containing hydroxyapatite coatings to the Candida albicans infection," in J. Microbiol. Methods, **Vol. 125**, 2016, pp. 12–18.

[26] *I. Fierascu, R. C. Fierascu, R. Somoghi, R. M. Ion, A. Moanta, S. M. Avramescu, C. M. Damian, L. M. Ditu,* "Tuned apatitic materials: Synthesis, characterization and potential antimicrobial applications," in Appl. Surf. Sci., **Vol. 438,** 2018, pp. 127-135.

[27] *J. Kolmas, E. Groszyk, D. Kwiatkowska-Różycka,* "Substituted Hydroxyapatites with Antibacterial Properties," in Biomed Res. Int., **Vol. 2014**, 2014, pp. 1–15.

[28] *D. Predoi, C. Popa, P. Chapon, A. Groza, S. Iconaru,* "Evaluation of the Antimicrobial Activity of Different Antibiotics Enhanced with Silver-Doped Hydroxyapatite Thin Films," in Materials (Basel), **Vol. 9, Iss.** 9, 2016, Article No. 778.

[29] *J. L. Falconer, D. W. Grainger*, "1.4 Silver Antimicrobial Biomaterials," in *Comprehensive Biomaterials II*, Elsevier, 2017, pp. 79–91.

[30] *A. Ortan, I. Fierascu, C. Ungureanu, R. C. Fierascu, S. M. Avramescu, O. Dumitrescu, C. E. Dinu-Pirvu*, "Innovative phytosynthesized silver nanoarchitectures with enhanced antifungal and antioxidant properties," in Appl. Surf. Sci., **Vol. 358,** Part B, 2015, pp. 540-548.

[31] *I. Cacciotti*, "Cationic and Anionic Substitutions in Hydroxyapatite," in *Handbook of Bioceramics and Biocomposites*, Springer International Publishing, 2016, pp. 145–211.

[32] *N. Rameshbabu, T. S. Sampath Kumar, T. G. Prabhakar, V. S. Sastry, K. V. G. K. Murty, K. Prasad Rao*, "Antibacterial nanosized silver substituted hydroxyapatite: Synthesis and characterization," in J. Biomed. Mater. Res. Part A**, Vol. 80A,** Iss. 3, 2007, pp. 581–591.

[33] *S. Kannan, J. M. G. Ventura, J. M. F. Ferreira*, "Synthesis and thermal stability of potassium substituted hydroxyapatites and hydroxyapatite/β-tricalciumphosphate mixtures," in Ceram. Int., **Vol. 33,** Iss. 8, 2007, pp. 1489-1494.

[34] *N. Iqbal, M. R. Abdul Kadir, N. H. Bin Mahmood, S. Iqbal, D. Almasi, F. Naghizadeh, H. R. Balaji, T. Kamarul*, "Characterization and biological evaluation of silver containing fluoroapatite nanoparticles prepared through microwave synthesis," in Ceram. Int., **Vol. 41**, Iss. 5, 2015, pp. 6470–6477.

[35] *A. Mocanu, G. Furtos, S. Rapuntean, O. Horovitz, C. Flore, C. Garbo, A. Danisteanu, G. Rapuntean, C. Prejmerean, M. Tomoaia-Cotisel*, "Synthesis; Characterization and antimicrobial effects of composites based on multi-substituted hydroxyapatite and silver nanoparticles," in Appl. Surf. Sci., **Vol. 298,** 2014, pp. 225-235.

[36] *Z.-Y. Qiu, C. Chen, X.-M. Wang, I.-S. Lee*, "Advances in the surface modification techniques of bone-related implants for last 10 years," in Regen. Biomater., **Vol. 1**, Iss. 1, 2014, pp. 67–79.

[37] *S. Bose, S. F. Robertson, A. Bandyopadhyay*, "Surface modification of biomaterials and biomedical devices using additive manufacturing," in Acta Biomater., **Vol. 66**, 2018, pp. 6–22.

[38] *M. Mozetič,* "Surface Modification to Improve Properties of Materials," in Materials, **Vol. 12**, Iss. 3, 2019, Article No. 441.

[39] *A. G. Gristina, P. T. Naylor, Q. Myrvik*, "The Race for the Surface: Microbes, Tissue Cells, and Biomaterials," in *Molecular Mechanisms of Microbial Adhesion*, Springer New York, 1989, pp. 177–211.

[40] *H. Chouirfa, H. Bouloussa, V. Migonney, C. Falentin-Daudré*, "Review of titanium surface modification techniques and coatings for antibacterial applications," in Acta Biomater., **Vol. 83**, 2019, pp. 37–54.

[41] *R. Bosco, J. Van Den Beucken, S. Leeuwenburgh, J. Jansen*, "Surface Engineering for Bone Implants: A Trend from Passive to Active Surfaces," in Coatings, **Vol. 2**, Iss. 3, 2012, pp. 95–119.

[42] *T.-T. Li, L. Ling, M.-C. Lin, H.-K. Peng, H.-T. Ren, C.-W. Lou, J.-H. Lin*, "Recent advances in multifunctional hydroxyapatite coating by electrochemical deposition," in J. Mater. Sci., **Vol. 55**, Iss. 15, 2020, pp. 6352–6374.

[43] *D. M. Vranceanu, T. Tran, E. Ungureanu, V. Negoiescu, M. Tarcolea, M. Dinu, A. Vladescu, R. Zamfir, A. C. Timotin, C. M. Cotrut*, "Pulsed electrochemical deposition of Ag doped hydroxyapatite bioactive coatings on Ti6Al4V for medical purposes," in UPB Sci. Bull. Ser. B Chem. Mater. Sci., **Vol. 80,** Iss. 1, 2018, pp. 173–184.

[44] *X. Lu, B. Zhang, Y. Wang, X. Zhou, J. Weng, S. Qu, B. Feng, F. Watari, Y. Ding, Y. Leng*, "Nano-Ag-loaded hydroxyapatite coatings on titanium surfaces by electrochemical deposition," in J. R. Soc. Interface, **Vol. 8**, Iss. 57, 2011, pp. 529–539.

[45] *V. K. Sharma, R. A. Yngard, Y. Lin*, "Silver nanoparticles: Green synthesis and their

antimicrobial activities," in Adv. Colloid Interface Sci., **Vol. 145**, Iss. 1–2, 2009, pp. 83–96.

[46] *Z. Feng, Y. Liao, M. Ye,* "Synthesis and structure of cerium-substituted hydroxyapatite," in J. Mater. Sci. Mater. Med., **Vol. 16**, Iss. 5, 2005, pp. 417–421.

[47] *Y. Huang, G. Song, X. Chang, Z. Wang, X. Zhang, S. Han, Z. Su, H. Yang, D. Yang, X. Zhang,* "Nanostructured Ag^{+}-substituted fluorhydroxyapatite-TiO_2 coatings for enhanced bactericidal effects and osteoinductivity of Ti for biomedical applications," in Int. J. Nanomedicine, **Vol. 13,** 2018, pp. 2665-2684.

[48] *Z. Geng, Z. Cui, Z. Li, S. Zhu, Y. Liang, Y. Liu, X. Li, X. He, X. Yu, R. Wang, X. Yang,* "Strontium incorporation to optimize the antibacterial and biological characteristics of silver-substituted hydroxyapatite coating," in Mater. Sci. Eng. C, **Vol. 58**, 2016, pp. 467–477.

[49] *F. Pishbin, V. Mouriño, J. B. Gilchrist, D. W. McComb, S. Kreppel, V. Salih, M. P. Ryan, A. R. Boccaccini,* "Single-step electrochemical deposition of antimicrobial orthopaedic coatings based on a bioactive glass/chitosan/nano-silver composite system," in Acta Biomater., **Vol. 9,** Iss.7, 2013, pp. 7469-7479.

[50] *P. Sikder, N. Koju, Y. Ren, V. K. Goel, T. Phares, B. Lin, S. B. Bhaduri,* "Development of single-phase silver-doped antibacterial CDHA coatings on Ti6Al4V with sustained release," in Surf. Coatings Technol., **Vol. 342,** 2018, pp. 105-116.

[51] *F. Variola, J. B. Brunski, G. Orsini, P. Tambasco de Oliveira, R. Wazen, A. Nanci,* "Nanoscale surface modifications of medically relevant metals: state-of-the art and perspectives," in Nanoscale, **Vol. 3**, Iss. 2, 2011, 335–353.

[52] *U. Meyer, A. Büchter, H. Wiesmann, U. Joos, D. Jones,* "Basic reactions of osteoblasts on structured material surfaces," in Eur. Cells Mater., **Vol. 9**, 2005, pp. 39–49.

[53] *J. Suwanprateeb, F. Thammarakcharoen, K. Wasoontararat, W. Chokevivat, P. Phanphiriya,* "Preparation and characterization of nanosized silver phosphate loaded hydroxyapatite by single step co-conversion process," in Mater. Sci. Eng. C, **Vol. 32**, Iss. 7, 2012, pp. 2122–2128.

[54] *T. Kobayashi, S. Ono, S. Hirakura, Y. Oaki, H. Imai,* "Morphological variation of hydroxyapatite grown in aqueous solution based on simulated body fluid," in Cryst. Eng. Comm., **Vol. 14**, Iss. 3, 2012, pp. 1143–1149.

[55] *C. M. Cotrut, A. Vladescu, M. Dinu, D. M. Vranceanu,* "Influence of deposition temperature on the properties of hydroxyapatite obtained by electrochemical assisted deposition," in Ceram. Int., **Vol. 44**, Iss. 1, 2018, pp. 669–677.

[56] *M. Markovic, B. O. Fowler, M. S. Tung,* "Preparation and comprehensive characterization of a calcium hydroxyapatite reference material," in J. Res. Natl. Inst. Stand. Technol., **Vol. 109,** Iss. 6, 2004, pp. 553-568.

[57] *K. P. Sanosh, M. C. Chu, A. Balakrishnan, Y. J. Lee, T. N. Kim, S. J. Cho,* "Synthesis of nano hydroxyapatite powder that simulate teeth particle morphology and composition," in Curr. Appl. Phys., **Vol. 9,** Iss. 6, 2009, pp. 1459-1462.

[58] *Baboian, R., Dean, S. W. J., Hack., H. P., Hibner, E. L.,Scully, J. R.* Corrosion Tests and Standards: Application and Interpretation - 2nd edition (ed. Baboian, R.) Ch. 3, 107–112 (ASTM International, **2005**).